



Measurement of the Forward-Backward Asymmetry of Top-Quark Pairs in the Dilepton Final State and Combination at CDF

The CDF Collaboration
URL <http://www-cdf.fnal.gov>
(Dated: June 10, 2015)

We measure the forward–backward asymmetry of top quark–antiquark pair events ($A_{\text{FB}}^{t\bar{t}}$) characterized by the rapidity difference of the top pairs (Δy_t) in the dilepton final state with the full CDF run II data, corresponding to an integrated luminosity of 9.1 fb^{-1} . The inclusive $A_{\text{FB}}^{t\bar{t}}$ is measured to be $A_{\text{FB}}^{t\bar{t}} = 0.12 \pm 0.13$, consistent with the NNLO standard model (SM) expectation of 0.095 ± 0.007 and the previous CDF result in the lepton + jets final state of 0.164 ± 0.047 . The combination of the CDF measurements of the inclusive $A_{\text{FB}}^{t\bar{t}}$ in both final states is 0.160 ± 0.045 , which is consistent with the NNLO SM prediction within 1.5σ . We also measure the differential $A_{\text{FB}}^{t\bar{t}}$ as a function of Δy_t , yielding $A_{\text{FB}}^{t\bar{t}}(|\Delta y_t| < 0.5) = 0.12 \pm 0.39$ and $A_{\text{FB}}^{t\bar{t}}(|\Delta y_t| > 0.5) = 0.13 \pm 0.17$. A linear fit to the differential $A_{\text{FB}}^{t\bar{t}}(|\Delta y_t|)$ with zero intercept yields a slope of $\alpha = 0.14 \pm 0.15$, consistent with the NNLO SM prediction of $0.114_{-0.012}^{+0.005}$ and the previous CDF determination in the lepton + jets final state of 0.253 ± 0.062 . The combined slope of $A_{\text{FB}}^{t\bar{t}}(|\Delta y_t|)$ in the two final states at CDF is $\alpha = 0.227 \pm 0.057$, which is 2.0σ larger than the NNLO SM prediction.

1. INTRODUCTION

The forward–backward asymmetry (A_{FB}) of the top quark–antiquark pair ($t\bar{t}$) system ($A_{\text{FB}}^{t\bar{t}}$) is a unique observable at the Tevatron, which quantifies the preference of top quarks to follow the proton direction, “forward”, instead of the anti-proton direction, “backward”. At leading order (LO) quantum chromodynamics (QCD) predicts no A_{FB} in $t\bar{t}$ production. All asymmetric effects come from the higher order perturbative QCD contributions as well as contributions from electroweak interactions [1]. The top quark A_{FB} program at the Tevatron exploits the proton–antiproton initial state to probe both the standard model (SM) at high precision and scenarios beyond the SM in ways not possible with the precision measurements of top physics at the LHC, where top pair production is dominated by gluon–gluon interactions and is symmetric along the beamline direction.

For the purpose of this analysis we take the $A_{\text{FB}}^{t\bar{t}}$ to be

$$A_{\text{FB}}^{t\bar{t}} = \frac{N(\Delta y_t > 0) - N(\Delta y_t < 0)}{N(\Delta y_t > 0) + N(\Delta y_t < 0)} \quad (1)$$

where N is the number of events, y is the rapidity of the top quark or antiquark (defined as $y = \frac{1}{2} \ln \frac{E+p_z}{E-p_z}$, with positive z defined along the proton direction), and $\Delta y_t = y_t - y_{\bar{t}}$. At next-to-leading order (NLO) the SM predictions for the inclusive value of $A_{\text{FB}}^{t\bar{t}}$ range from 0.05 to 0.125, as discussed in Ref. [2] and references therein, while we consider $A_{\text{FB}}^{t\bar{t}} = 0.088 \pm 0.006$ [1] (with the conventional renormalization scale ($\mu_R \sim m_t$) and with the LO electroweak corrections) to be our benchmark NLO value. We will compare typically with the next-to-next-leading order (NNLO) calculation of $A_{\text{FB}}^{t\bar{t}} = 0.095 \pm 0.007$ [3]. If particles beyond the SM are considered, the A_{FB} can be drastically changed (higher or lower) because of interference among diagrams [4]. The asymmetry is greatly enhanced in certain kinematic regions, thus the measurements of the differential asymmetries are also of great importance. The $A_{\text{FB}}^{t\bar{t}}$ as a function of $|\Delta y_t|$ can be phenomenologically characterized with the slope (α) of a linear function with zero offset. An NNLO calculation estimates the slope to be $0.114_{-0.012}^{+0.005}$ [3, 5].

On the experimental side, the measurement of the inclusive $A_{\text{FB}}^{t\bar{t}}$ with CDF data corresponding to 9.4 fb^{-1} of integrated luminosity in the lepton+jets final state [6] shows a value of 0.164 ± 0.047 which is 1.5σ higher result than the NNLO SM prediction. The same measurements with D0 data corresponding to 9.7 fb^{-1} of integrated luminosity in the lepton+jets [7] and dilepton final state [8] show results of 0.106 ± 0.030 and 0.180 ± 0.086 , which are consistent with the NNLO SM prediction.¹ The differential measurements of the $A_{\text{FB}}^{t\bar{t}}$ show the same trend. The differential $A_{\text{FB}}^{t\bar{t}}$ as a function of $|\Delta y_t|$ measurement by CDF in the lepton+jets final state [6] shows a slope of 0.253 ± 0.062 , which is 2.2σ higher than the NNLO SM prediction [3, 5]. The same measurement carried out at D0 in the lepton+jets final state [7] yields a slope of 0.154 ± 0.043 which is consistent with the NNLO SM prediction. We note that the differential $A_{\text{FB}}^{t\bar{t}}$ as a function of the invariant mass of the top pairs measured at CDF also shows a mild tension with the NLO SM prediction, while the measurement at D0 shows consistency.

We note a few other relevant results before the description of our analysis and results. A more detailed study of the cross section of the $t\bar{t}$ system as a function of the production angle of the top quark in the $t\bar{t}$ rest frame (θ^*) was performed in the lepton+jets final state at CDF [9]. The differential cross section $\frac{d\sigma}{d\cos\theta^*}$ has been decomposed in terms of Legendre polynomials and it was determined that the “excess” in the $A_{\text{FB}}^{t\bar{t}}$ measurement in this channel is due to the coefficient of the first order Legendre polynomials, which is a term linearly dependent on $\cos\theta^*$. This motivates an *ad hoc* method of simulating variations in $A_{\text{FB}}^{t\bar{t}}$ in an SM-like scenario, as will be described and used in Sec. 4. This method is needed because there is no free parameter in the SM which governs $A_{\text{FB}}^{t\bar{t}}$. We also note that the consistency of the measurements with the SM can also be probed in alternative ways. For example, the leptons from the top cascade decays carry directional information from their parent top quarks, and thus the A_{FB} measurements of the leptons (A_{FB}^ℓ and $A_{\text{FB}}^{\ell\bar{\ell}}$) serve as complementary measurements to $A_{\text{FB}}^{t\bar{t}}$ [10] and mostly show agreement with the SM, with the CDF lepton+jets result showing similar amounts of disagreement as in the $A_{\text{FB}}^{t\bar{t}}$.

This note summarizes the inclusive and differential $A_{\text{FB}}^{t\bar{t}}$ measurements in the dilepton final state as well as their combination with the lepton+jets results. It uses the full dataset collected during Tevatron Run II, corresponding to an integrated luminosity of 9.1 fb^{-1} , and is thus the final word from CDF on $A_{\text{FB}}^{t\bar{t}}$ measurements. This measurement supercedes the previous $A_{\text{FB}}^{t\bar{t}}$ measurement in the dilepton final state with the data of 5.1 fb^{-1} [11] with a larger

¹ All the Tevatron legacy results of the inclusive $A_{\text{FB}}^{t\bar{t}}$ measurements, including the result described in this note, are summarized in Fig. 12.

data size, better background rejection and estimation techniques, better signal modeling (NLO vs. LO), an improved top-quark-pair reconstruction, optimized selection criteria and weighting schemes, and a more sophisticated unfolding procedure.

The structure of this note is to present the new dilepton analysis, and then the combination. The dilepton analysis starts with the same dataset as the legacy measurements of the A_{FB}^ℓ in the same final state [12], mentioned in Sec. 2. In Sec. 3 we describe the likelihood-based event reconstruction for the kinematics of the $t\bar{t}$ pairs. In Sec. 4 we describe the parton-level $A_{\text{FB}}^{t\bar{t}}$ extraction procedure. In Sec. 5 we specify the optimization procedure and then present the validation of the full methodology in Sec. 6. A final set of systematic uncertainties is estimated in Sec. 7. We present the final measurements of both the inclusive $A_{\text{FB}}^{t\bar{t}}$, as well as the differential measurement of $A_{\text{FB}}^{t\bar{t}}$ as a function of $|\Delta y_t|$ in Sec. 8. The combination of the dilepton results and the lepton+jets results is shown in Sec. 9, with our final conclusions in 10.

2. EVENT SELECTION AND BACKGROUND ESTIMATION

The baseline event selection criteria are unchanged from those used in the A_{FB}^ℓ measurement, documented in Ref. [12]. We require two oppositely charged leptons, two or more narrow clusters of energy deposits in the calorimeters corresponding to collimated clusters of incident hadrons (jets), and an imbalance in the total event transverse momentum (\cancel{E}_T). A number of other kinematic cuts are made to enhance the signal purity, to ensure good measurement of the events, and to ensure our estimates of the backgrounds are robust.

The signal and backgrounds estimations are also the same as those used in Ref. [12]. The $t\bar{t}$ signal is modeled with the NLO MC generator POWHEG [13]. The background sources include the production of a Z boson or a virtual photon with jets ($Z/\gamma^* + \text{jets}$), production of a W boson with jets ($W + \text{jets}$), diboson production (WW , WZ , ZZ , and $W\gamma$), and $t\bar{t}$ production where one of the W bosons from the top-quark pair decays hadronically and one jet from bottom-quark hadronization or W -boson hadronic decay is misidentified as a lepton ($t\bar{t}$ nondilepton). Most sources of the background are modeled using MC with the full detector simulation [14], while the $W + \text{jets}$ background is modeled using a data-driven technique. The total expected event count is 569 ± 40 , with an expected signal purity of 72%. More detailed comparisons of the data with predictions will be presented in Sec. 6 after the final optimization selection criteria are applied.

3. TOP RECONSTRUCTION

An example Feynman diagram of a $t\bar{t}$ event in the dilepton final state ($t\bar{t} \rightarrow \ell^+ \ell^- \nu \bar{\nu} b \bar{b}$) is shown in Fig. 1. Since the primary goal is to measure the asymmetry characterized by Δy_t , we begin the analysis by attempting to reconstruct the kinematics of the top and the antitop on an event-by-event basis. The kinematic reconstruction is done by combining the final-state decay products together to form first two W bosons and then two top quarks. This involves pairing each lepton with some portion of the \cancel{E}_T to reconstruct a W -boson, and then pairing each reconstructed W with one of the jets to form a top. The primary challenges of the reconstruction technique are to choose the correct lepton-jet pairing, to solve for the neutrino momentum within each pairing, and to determine the best $t\bar{t}$ kinematic solution when multiple solutions exist.

We follow the lead of previous methods of reconstructing the top kinematics, which aim to identify the most probable solution with a likelihood-based algorithm [11]. To make better use of the information, we scan over the full kinematically allowed parameter space and obtain the probability density distribution of the kinematics of the $t\bar{t}$ system for each potential solution. We note at the outset that this full set of information will be used in the unfolding method used to take the reconstructed events to parton-level measurements described in the next section to reduce the uncertainties. Additional event selection criteria, partially based on the reconstruction likelihoods, will be used to optimize the sensitivity of the analysis by rejecting poorly reconstructed top pairs, as well as rejecting non-top-pair events.

In order to resolve the four-momenta of both the top quark and the antiquark, we need to solve for the four-momenta

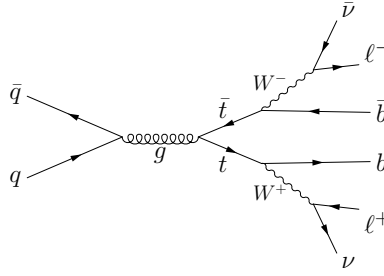


FIG. 1: An example Feynman diagram of the top pair production and decay in the dilepton final state.

of all the final state particles, constrained by the energy-momentum conservation equations:

$$\begin{aligned}
 M_{\ell^+\nu}^2 &= (E_{\ell^+} + E_{\nu})^2 - (\vec{p}_{\ell^+} + \vec{p}_{\nu})^2 = M_W^2 \\
 M_{\ell^-\bar{\nu}}^2 &= (E_{\ell^-} + E_{\bar{\nu}})^2 - (\vec{p}_{\ell^-} + \vec{p}_{\bar{\nu}})^2 = M_W^2 \\
 M_{\ell^+\nu b}^2 &= (E_{\ell^+} + E_{\nu} + E_b)^2 - (\vec{p}_{\ell^+} + \vec{p}_{\nu} + \vec{p}_b)^2 = M_t^2 \\
 M_{\ell^-\bar{\nu}\bar{b}}^2 &= (E_{\ell^-} + E_{\bar{\nu}} + E_{\bar{b}})^2 - (\vec{p}_{\ell^-} + \vec{p}_{\bar{\nu}} + \vec{p}_{\bar{b}})^2 = M_t^2 \\
 (\vec{p}_{\nu} + \vec{p}_{\bar{\nu}})_x &= \cancel{E}_x \\
 (\vec{p}_{\nu} + \vec{p}_{\bar{\nu}})_y &= \cancel{E}_y.
 \end{aligned} \tag{2}$$

The basic ideas and assumptions of the top reconstruction used in this analysis are:

1. The two opposite-charged leptons are measured with high precision at CDF. We take the measured momenta of the charged leptons as their true values (i.e., negligible uncertainties).
2. We assume the two jets with the largest E_T (and $|\eta| < 2.5$) come from the hadronization of the b and the \bar{b} quarks. The directions of the jets are assumed to correctly indicate the directions of their original quarks. Using MC techniques, the jet E_T values (after the standard corrections [15]) are further corrected so that the mean of the jet E_T matches the b -quark E_T [16] from POWHEG, and in the reconstruction phase the jet E_T are allowed to float according to their mean values and expected resolutions. In addition, we fix the masses of the jets to be $4.66 \text{ GeV}/c^2$ [17].
3. Each charged lepton needs to be paired with a b/\bar{b} quark to form a t/\bar{t} quark (together with the undetected neutrinos). Since there is no perfect separation between jets from b quarks and jets from \bar{b} quarks, we consider both lepton-jet pairings in the reconstruction, but will use techniques to reduce the contamination of the measurement from wrong pairings.
4. While the two neutrinos in the final state are not detected, resulting in six unknown variables (assuming massless neutrinos), the sum of the transverse momenta of the two neutrinos produces an imbalanced- p_T of the event ($\vec{\cancel{E}}_T$). However, since the two measured components of $\vec{\cancel{E}}_T$ (\cancel{E}_x and \cancel{E}_y) have large resolutions, the vector sum of the transverse momenta of the neutrinos are allowed to float in the reconstruction according to the measured mean values and resolutions of $\vec{\cancel{E}}_T$.
5. In all calculations we include four constraints in the $t\bar{t}$ system: the two W -boson masses ($m_W = 80.4 \text{ GeV}/c^2$) and the two top-quark masses ($m_t = 172.5 \text{ GeV}/c^2$) [17].

With these assumptions, for each of the two lepton-jet pairings, there are ten unknown variables in the $t\bar{t}$ dilepton final state (six from the momenta of the neutrinos, two from the floating jet E_T and two from the floating $\vec{\cancel{E}}_T$) and two choices of lepton-jet pairings. On the other hand, we have six constraints from Eq. 2 (the two W -boson masses, the two top-quark masses, and the constraints from \cancel{E}_x and \cancel{E}_y separately). Thus, for each event the variables and constraints form two under-constrained systems with degenerate solutions in a four-dimensional parameter space. The strategy of the top reconstruction in this analysis is to scan these two four-dimensional parameter spaces and to assign a likelihood to each point of the phase space based on the measured objects and their uncertainties. Additional information about the expected kinematics, as estimated using POWHEG, will also be used to improve the performance of the reconstruction.

With these sets of assumptions, the kinematics of a $t\bar{t}$ event can be characterized as a function of the momenta of the neutrinos (\vec{p}_{ν} and $\vec{p}_{\bar{\nu}}$) and the transverse energy of the b/\bar{b} quarks ($E_{T,b}$ and $E_{T,\bar{b}}$). The quantities \vec{p}_{ν} , $\vec{p}_{\bar{\nu}}$, $E_{T,b}$

and $E_{T,\bar{b}}$ are not independent of each other, but are subject to the constraints of Eq. 2. In the kinematically allowed region, we define the following likelihood to quantify the goodness of a solution:

$$\begin{aligned} \mathcal{L}(\vec{p}_\nu, \vec{p}_{\bar{\nu}}, E_{T,b}, E_{T,\bar{b}}) &= P(p_{z,t\bar{t}}) \times P(p_{T,t\bar{t}}) \times P(m_{t\bar{t}}) \\ &\times \frac{1}{\sigma_{\text{jet1}}} \exp\left(-\frac{1}{2} \left(\frac{E_{T,\text{jet1}} - E_{T,b}}{\sigma_{\text{jet1}}}\right)^2\right) \times \frac{1}{\sigma_{\text{jet2}}} \exp\left(-\frac{1}{2} \left(\frac{E_{T,\text{jet2}} - E_{T,\bar{b}}}{\sigma_{\text{jet2}}}\right)^2\right) \\ &\times \frac{1}{\sigma(\vec{E}_x)} \exp\left(-\frac{1}{2} \left(\frac{\vec{E}_x - (\vec{p}_\nu + \vec{p}_{\bar{\nu}})_x}{\sigma(\vec{E}_x)}\right)^2\right) \times \frac{1}{\sigma(\vec{E}_y)} \exp\left(-\frac{1}{2} \left(\frac{\vec{E}_y - (\vec{p}_\nu + \vec{p}_{\bar{\nu}})_y}{\sigma(\vec{E}_y)}\right)^2\right), \end{aligned} \quad (3)$$

where $P(p_{z,t\bar{t}})$, $P(p_{T,t\bar{t}})$, and $P(m_{t\bar{t}})$ are the probability density functions of each parameter obtained with the dilepton candidate events in the $t\bar{t}$ MC sample generated by POWHEG [13], the two $E_{T,\text{jet}}$ values are the transverse energies of the two jets, the two σ_{jet} values are the resolution of the jet transverse energies estimated with the POWHEG MC sample with full CDF detector simulation [14], and $\vec{E}_{x,y}$ are the x and y components of the measured \vec{E}_T , and $\sigma(\vec{E}_{x,y})$ are the resolution of $\vec{E}_{x,y}$ estimated with the same POWHEG MC sample.

We employ a Markov-chain Monte Carlo (MCMC) method [18] to effectively scan the parameter space with each of the two lepton-jet pairings and map out the probability distributions of the parameters of interest (Δy_t in this analysis) with marginalization. The package we use for the MCMC method is *Bayesian Analysis Toolkit* (BAT) [19]. To make the best use of the available information we use the full probability density distributions obtained from the MCMC method in our parton-level $A_{\text{FB}}^{t\bar{t}}$ extraction method (described in the next section) and weight the two lepton-jet pairings based on the maximum likelihood achieved in each of the two pairings ($L_{\text{max},1,2}$). The weight of each lepton-jet pairing is determined by

$$w_{1,2} = \frac{L_{\text{max},1,2}}{L_{\text{max},1} + L_{\text{max},2}} \quad (4)$$

With these set of choices we find that the resolution of the top reconstruction algorithm is of the order of 0.5 in Δy_t . We will show the final performance of the algorithm in Sec. 6, after the optimization procedure described in Sec. 5.

4. EXTRACTING PARTON-LEVEL $A_{\text{FB}}^{t\bar{t}}$

Because of the limited acceptance and the efficiency of the detector, the imperfect resolution of the Δy_t reconstruction and the background contributions, a sophisticated procedure is needed to turn the Δy_t distribution into a parton-level A_{FB} measurement. We introduce a Bayesian model, again implemented with BAT, to correct the Δy_t distribution (taking into account the correlations among the measured values) and extract the $A_{\text{FB}}^{t\bar{t}}$ values at the parton level from data. It allows us to measure both the inclusive $A_{\text{FB}}^{t\bar{t}}$ as well as $A_{\text{FB}}^{t\bar{t}}$ as a function of $|\Delta y_t|$.

To develop and validate the extraction procedure, we use a series of samples with various $A_{\text{FB}}^{t\bar{t}}$ values. Since there is no free parameter in the SM which causes the $A_{\text{FB}}^{t\bar{t}}$ to vary, we follow a hint suggested by the measurement of the top quark differential cross section ($\frac{d\sigma}{d\cos\theta^*}$) in terms of Legendre polynomials in the lepton+jets final state [9], which suggests that the higher-than-predicted $A_{\text{FB}}^{t\bar{t}}$ is due to an extra contribution to $\frac{d\sigma}{d\cos\theta^*}$ that depends linearly on $\cos\theta^*$ (a_1). We create a series of MC samples with various $A_{\text{FB}}^{t\bar{t}}$ by reweighting the POWHEG MC sample with various extra linear contributions ($-0.3 < \text{extra } a_1 < 0.5$) to $\frac{d\sigma}{d\cos\theta^*}$, corresponding to $-0.1 < A_{\text{FB}}^{t\bar{t}} < 0.3$.

In this analysis, we use four bins of Δy_t at both parton level as well as after reconstruction, with similar expected number of $t\bar{t}$ events per bin. They are $(-\infty, -0.5)$, $(-0.5, 0)$, $(0, 0.5)$ and $(0.5, \infty)$ (designated bin 1, 2, 3, and 4, respectively). The parton-level inclusive $A_{\text{FB}}^{t\bar{t}}$ is expressed as

$$A_{\text{FB}}^{t\bar{t}}(\text{incl.}) = \frac{\text{parton}[3] + \text{parton}[4] - \text{parton}[1] - \text{parton}[2]}{\text{parton}[3] + \text{parton}[4] + \text{parton}[1] + \text{parton}[2]}, \quad (5)$$

where $\text{parton}[p]$ represents the parton-level event count in the p -th bin. The Bayesian model is expressed as

$$\exp[r] = \sum_{p=1}^4 \text{parton}[p] \cdot \text{eff}[p](A_{\text{FB}}^{t\bar{t}}) \cdot \det[p][r] + \text{bkg}[r], \quad (6)$$

where

- $\text{parton}[p]$ is the hypothetical underlying parton-level bin count,

- $\text{exp}[r]$ is the expected number of events in the r -th bin after the top reconstruction for a particular set of $\text{parton}[p]$,
- $\text{eff}[p](A_{\text{FB}}^{t\bar{t}})$ represents the efficiency in the p -th bin at parton-level to account for the acceptance imposed by the detector coverage and the efficiency caused by the event selections (which turns out to be a function of the parton-level $A_{\text{FB}}^{t\bar{t}}$),
- $\text{det}[p][r]$ represents the smearing matrix to account for the imperfect detector resolution and the smearing caused by the top reconstruction procedure (which shows no substantive change as a function of the input $A_{\text{FB}}^{t\bar{t}}$), and
- $\text{bkg}[r]$ is the expected background contribution in r -th bin.

The $\text{eff}[p](A_{\text{FB}}^{t\bar{t}})$ term is estimated with the reweighted POWHEG MC samples, and the $\text{det}[p][r]$ term is estimated with the nominal POWHEG MC sample. The observed bin count from data ($\text{obs}[r]$) is compared with the expectation $\text{exp}[r]$ with correlations among bins estimated with the POWHEG $t\bar{t}$ MC sample.

To allow for the use of well-motivated priors, we re-parametrize the Bayesian model with four parameters:

1. $\text{ntot} = \sum_{p=1}^4 \text{parton}[p]$ is the total number of signal events, with a uniform, non-negative prior probability distribution
2. $\text{Ain} = \frac{\text{parton}[3]-\text{parton}[2]}{\text{parton}[3]+\text{parton}[2]} = A_{\text{FB}}^{t\bar{t}}(|\Delta y_t| < 0.5)$ is the asymmetry of bins 2 and 3, with a uniform prior in $(-1, 1)$
3. $\text{Aout} = \frac{\text{parton}[4]-\text{parton}[1]}{\text{parton}[4]+\text{parton}[1]} = A_{\text{FB}}^{t\bar{t}}(|\Delta y_t| > 0.5)$ is the asymmetry of bins 1 and 4, with a uniform prior in $(-1, 1)$
4. $\text{Rin} = \frac{\text{parton}[2]+\text{parton}[3]}{\text{ntot}}$ is the fraction of events in the inner two bins, with a uniform prior in $(0, 1)$.

With this new parametrization, the inclusive $A_{\text{FB}}^{t\bar{t}}$ in Eq. 5 can be written as

$$A_{\text{FB}}^{t\bar{t}} = \text{Rin} \cdot \text{Ain} + (1 - \text{Rin}) \cdot \text{Aout} \quad (7)$$

The posterior probability distribution of all parameters of interest ($A_{\text{FB}}^{t\bar{t}}$ (incl.), $A_{\text{FB}}^{t\bar{t}}(|\Delta y_t| < 0.5)$ and $A_{\text{FB}}^{t\bar{t}}(|\Delta y_t| > 0.5)$) are obtained by marginalizing out all other parameters. The parameters and their statistical uncertainties are extracted by fitting a Gaussian function to the central region of the posterior distributions.

The extraction procedure is validated and the uncertainties are estimated using two sets of 5k pseudo-experiments. One set of pseudo-experiments is generated by randomly picking events from the nominal POWHEG MC sample with the number of events matching the signal expectation in data, and the second set of pseudo-experiments is generated by randomly picking events from both the signal and the backgrounds. Each pseudo-experiment is processed with the nominal correction procedure. The pseudo-experiments are used to test for potential bias as well as to determine the expected statistical uncertainty with signal only, and the total statistical uncertainty when the backgrounds are included (but not taking into account systematic uncertainties on the backgrounds). As we will show in Sec. 6, no bias is observed. The expected total statistical uncertainty before optimization for the inclusive measurement in data, estimated as the RMS of the observed values from the second set of pseudo-experiments, is around 0.12, and is the dominant uncertainty. As in Ref. [12], we take the systematic uncertainty due to the uncertainty on the background normalization and shape to be equal to the difference in quadrature between the total statistical uncertainty and the signal-only statistical uncertainty. The background systematic uncertainty is estimated to be 0.06 before the optimization we describe in Sec. 5. Additional uncertainties will be described in Sec. 7.

Before showing any figures for this procedure, in the next section we will describe the optimization procedure we perform for the inclusive $A_{\text{FB}}^{t\bar{t}}$ where we minimize the expected total statistical uncertainty + the background systematic uncertainty, as other uncertainties are expected to be small. We will summarize the validation of the correction procedure in Sec. 6 after the optimization.

5. OPTIMIZATION

The top reconstruction algorithm and the parton-level $A_{\text{FB}}^{t\bar{t}}$ extraction procedures are designed to allow for an optimization strategy that minimizes the expected uncertainties. Besides the statistical uncertainty due to the limited data sample size, the uncertainty of the parton-level $A_{\text{FB}}^{t\bar{t}}$ receives a contribution from the resolution of the reconstruction, especially the events with Δy_t reconstructed far away from their parton-level values. The usual reconstruction method of picking the maximum-likelihood solution suffers from two primary problems: 1) the algorithm sometimes

selects the wrong lepton-jet pairing and 2) the algorithm sometimes gives the highest likelihood values to a set of wrong values of the parameter choices within the right lepton-jet pairing. To ameliorate these problems we keep the full probability distributions and weight both lepton-jet pairings instead of picking the maximum-likelihood solution, which we find gives better resolution for the $A_{\text{FB}}^{t\bar{t}}$ measurement. We perform further optimization by incorporating additional event selection requirements to reject badly reconstructed lepton-jet pairings and giving larger weights to pairings that are more likely to be the correct ones. We only optimize based on the expected uncertainties of the inclusive $A_{\text{FB}}^{t\bar{t}}$ measurement.

For wrong lepton-jet pairings or background events the top reconstruction algorithm sometimes pulls the jet E_T far away from the measured value to try to make a valid $t\bar{t}$ pair. We quantify this deviation using the parameter $jd = \frac{E_{T,\text{jet}} - E_{T,b}}{\sigma_{jet}}$, and for simplicity examine only the peak position of the jd distribution (jd_{peak}) for each jet. We reject any lepton-jet pairing with $\sqrt{jd_{1,\text{peak}}^2 + jd_{2,\text{peak}}^2} > jd\text{-cut}$, and reject the event if both lepton-jet pairings are rejected. It turns out that this cut is efficient in rejecting both badly reconstructed signal events as well as background events, in particular from W +jets sources.

The track-weighted jet charge ($Q_{\text{jet}1,2}$) is correlated with the charge of its original quark [20] and can provide additional separation between the b -quark and the \bar{b} -quark, thus helping identify the correct lepton-jet pairing. This technique was recently used in the measurement of the A_{FB} of $b\bar{b}$ at high invariant mass of the $b\bar{b}$ pairs at CDF [21]. While the track-weighted jet charge suffers from limited reconstruction efficiency ($\sim 90\%$), B - \bar{B} mixing, B -meson cascade decays, and the bias created by the detector material and track reconstruction, it still provides a worthwhile improvement in the resolution of the $A_{\text{FB}}^{t\bar{t}}$. For each event we examine the sign of $\Delta Q = Q_{\text{jet}1} - Q_{\text{jet}2}$, after assigning $Q_{\text{jet}} = 0$ for jets without valid reconstructed charges for simplicity; positive ΔQ suggests that jet1 is from the \bar{b} -quark and jet2 is from the b -quark, and vice versa. The case $\Delta Q = 0$ indicates that the jet charge doesn't provide distinguishing power between the b/\bar{b} quarks. To use this information we introduce a global jet-charge probability weight w_Q that quantifies the probability that the jet charge gives the correct lepton-jet pairing. We then amend the L_{max} of the two pairings used in Eq. 4 to $L_{\text{max}} * w_Q$ if ΔQ suggests this pairing and $L_{\text{max}} * (1 - w_Q)$ if ΔQ suggests otherwise, and proceed with Eq. 4 in determining the weights of the two pairings. We optimize for the value of w_Q .

A third way to improve the resolution is to reject the lepton-jet pairings with high $m_{l\bar{b}}^2$ which are unlikely to be from a top decay, where $m_{l\bar{b}}$ is the invariant mass of the lepton+ b -quark system [22]. The optimization is set to reject any lepton-jet pairings with $m_{l\bar{b}}^2 > m_{l\bar{b}}^2\text{-cut}$, and reject the event if both lepton-jet pairings are rejected.

Finally, we note that events with a lepton appearing too close to a jet either don't reconstruct well or are likely to be from a W +jets event where a b -jet is reconstructed as a lepton and a jet [23]. This effect is quantized as the minimum ΔR between any lepton and any jet ($\Delta R_{\text{min}}(\text{lepton}, \text{jet})$). We optimize for a cut on $\Delta R_{\text{min}}(\text{lepton}, \text{jet})$ as it helps reject W +jets background events without significantly reducing the number of the well-reconstructed $t\bar{t}$ events.

The minimization of all cut/weight values are done simultaneously and Table I shows the optimum values for all cuts and weights. Figure 2 shows the expected uncertainties as functions of the cut and weight values with other values fixed at the optimum points. We proceed with the analysis with these optimized cuts and weights. The signal efficiency of the top reconstruction quality cuts is 95% with a background rejection of 40% relative to the baseline cuts. The minimum expected uncertainties achieved are 0.106 for the signal-only statistical uncertainty, 0.114 for the statistical uncertainty of signal and backgrounds (total statistical uncertainty), and 0.121 for the statistical and background systematic uncertainty. For the differential measurement we find the expected total statistical uncertainties of 0.34 for $A_{\text{FB}}^{t\bar{t}}(|\Delta y_t| < 0.5)$ and 0.16 for $A_{\text{FB}}^{t\bar{t}}(|\Delta y_t| > 0.5)$.

Optimum cut and weight	
jd-cut	3.5
w_Q	0.7
$m_{l\bar{b}}^2 > m_{l\bar{b}}^2\text{-cut}$	24000 (GeV ²)
$\Delta R_{\text{min}}(\text{lepton}, \text{jet})\text{-cut}$	0.2

TABLE I: Summary of the cut and weight values used to optimize the expected uncertainties in the measurement of the inclusive $A_{\text{FB}}^{t\bar{t}}$.

6. VALIDATION

The expected numbers of events from all SM sources along with the observed number of events, passing all the top dilepton event selections and the top reconstruction quality selections, are summarized in Table II. The distribution of $p_{T,t\bar{t}}$, $p_{z,t\bar{t}}$ and $m_{t\bar{t}}$ from data are shown in Fig. 3 together with the comparison with the SM predictions using

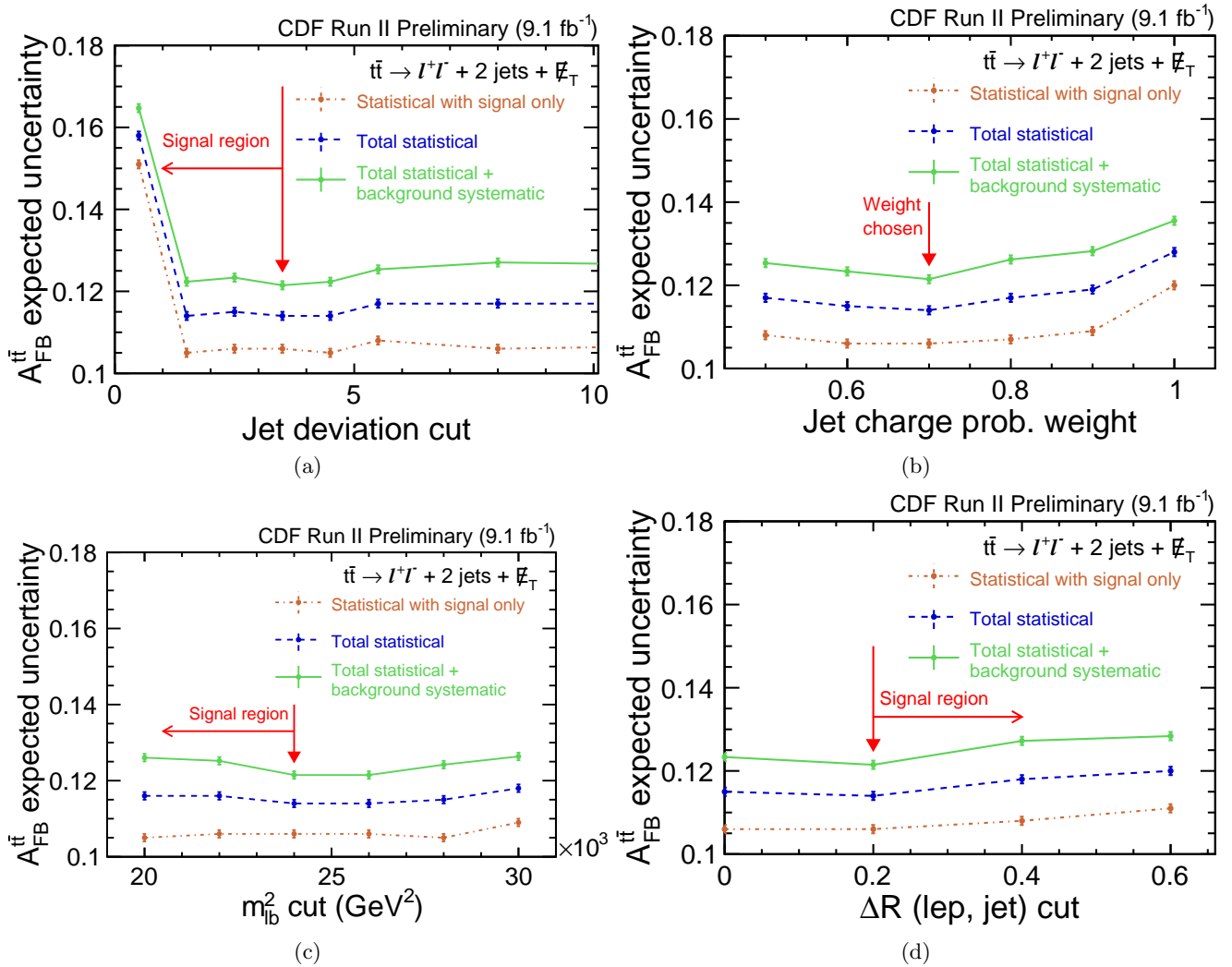
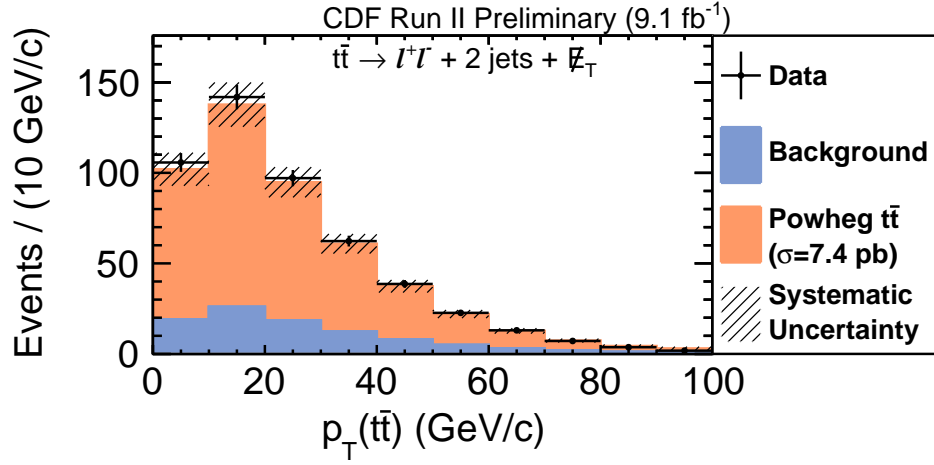
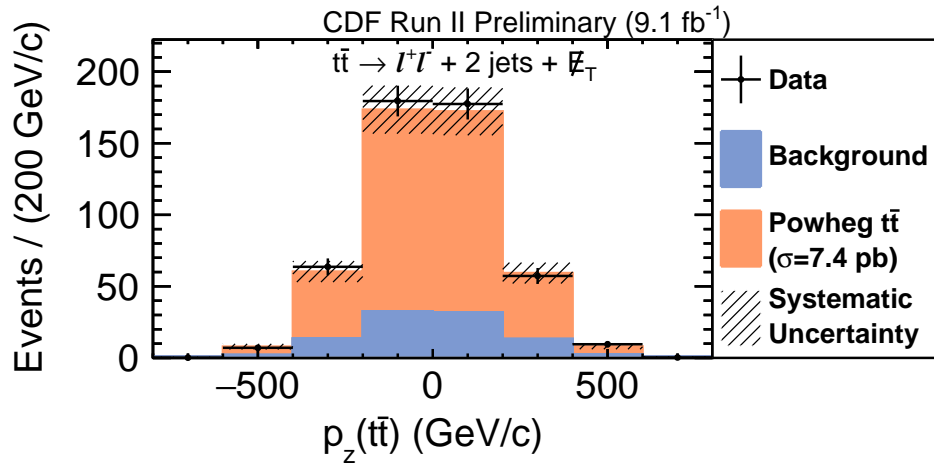
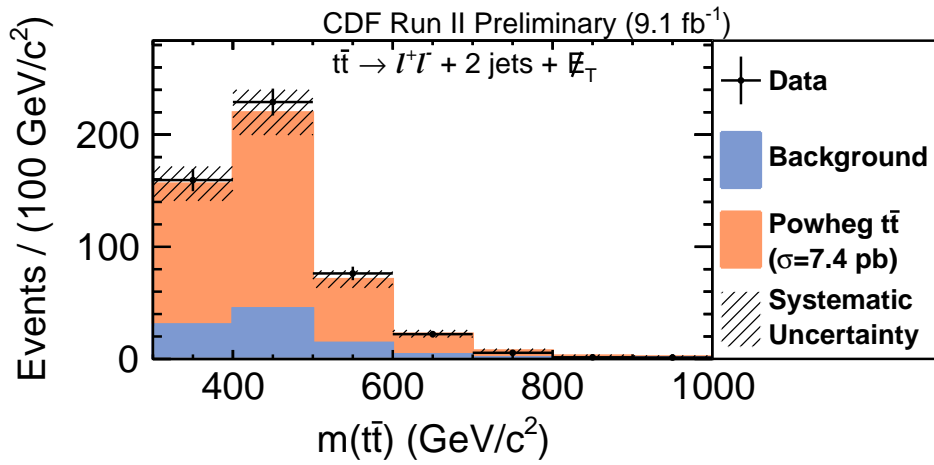


FIG. 2: The expected uncertainties as a function of the four optimization parameters. In each plot is shown the statistical uncertainty for signal only (brown line), statistical uncertainty for signal + backgrounds (total statistical uncertainty, blue dashed line) and total statistical + background systematic uncertainty (green line). The optimum values are based on the minimum point of the green line, as marked with the red arrows on the plots, and summarized in Table I. For each plot, all other values are held at their optimal values as summarized in Table I.

POWHEG. In all cases the agreement between data and the predictions is good. The reconstructed Δy_t is shown in Fig. 4. The A_{FB}^{tt} will be extracted from this distribution.

Figure 5 shows the reconstruction resolution ($\Delta y_t(\text{reconstructed}) - \Delta y_t(\text{generated})$) estimated for events from the POWHEG MC sample. We note that 61% of the time the Δy_t is reconstructed within 0.5 of its true value. The detector smearing matrix ($\det[p][r]$ in Eq. 6) is shown in Fig. 6. The efficiencies in the four bins are characterized as linear functions of the A_{FB}^{tt} summarized in Fig. 7.

We test the unfolding procedure with the reweighted POWHEG samples. The results are shown in Fig. 8. The error bars correspond to the statistical uncertainties based on the whole MC sample ($\sim 70\text{k}$ events after event selection criteria). There is no bias observed. In addition, we test the unfolding algorithm with the LO SM calculations (PYTHIA [24], ALPGEN [25] and HERWIG [26]) as well as a series of benchmark BSM scenarios (t-channel Z' [27], and a variety of models containing an axigluon of various mass and handedness, including 425 GeV Axi [28], 200 GeV AxiL/A/R [29], and 1.8/2.0 TeV Axi [30]). The results can be found in Fig. 9. We do not expect the unfolding procedure to work perfectly with all BSM scenarios as the kinematics can be very different from the SM predictions. However, we note that the biggest deviation is 0.08 which is small compared to the dominant uncertainty of 0.11 from limited statistics. We take the difference between the generated A_{FB}^{tt} and the measured A_{FB}^{tt} with the PYTHIA MC sample (0.02) as the systematic uncertainty for the unfolding procedure to cover the potential bias caused by the

(a) $p_{T,t\bar{t}}$ (b) $p_{z,t\bar{t}}$ (c) $m_{t\bar{t}}$ FIG. 3: The distribution of $p_{T,t\bar{t}}$, $p_{z,t\bar{t}}$, and $m_{t\bar{t}}$ from data compared with the SM expectations.

CDF Run II Preliminary (9.1 fb ⁻¹)	
Expected and observed events ($t\bar{t} \rightarrow l^+l^- + 2\text{jets} + \cancel{E}_T$)	
Source	Events
Diboson	26±5
Z/γ*+jets	37±4
W+jets	28±9
$t\bar{t}$ non-dilepton	5.3±0.3
Total background	96±18
Signal $t\bar{t}$ ($\sigma = 7.4$ pb)	386±18
Total SM expectation	482±36
Observed	495

TABLE II: The expected and observed number of events, passing all the top dilepton event selections and the top reconstruction quality selections.

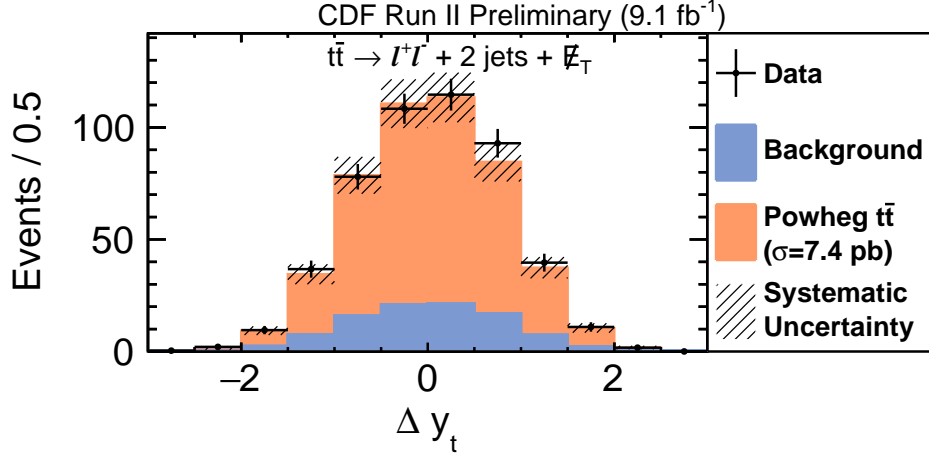


FIG. 4: The distribution of Δy_t from data compared with the SM expectations.

NLO SM assumption we made in the top reconstruction procedure and the unfolding procedure.

Figure 10 shows a comparison of $A_{\text{FB}}^{t\bar{t}}(|\Delta y_t| < 0.5)$ and $A_{\text{FB}}^{t\bar{t}}(|\Delta y_t| > 0.5)$ between the measured values and the input ones, for the reweighted POWHEG MC samples. The error bars again correspond to the statistical uncertainties with the full POWHEG MC sample. We note that the deviation between the measured values and the generated values in the worst case is consistent with their statistical uncertainties, and negligible compared to the expected statistical uncertainties from data. We do not attempt to fix this potential, yet negligible, bias and simply take the difference as a systematic uncertainty.

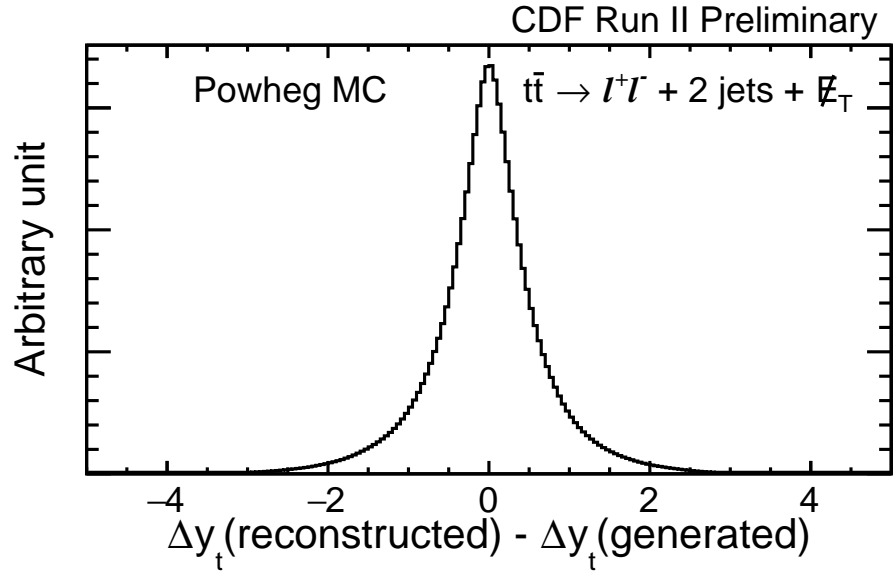


FIG. 5: The distribution of $\Delta y(\text{reconstructed}) - \Delta y(\text{generated})$ from events in the nominal POWHEG MC after all the event selection criteria.

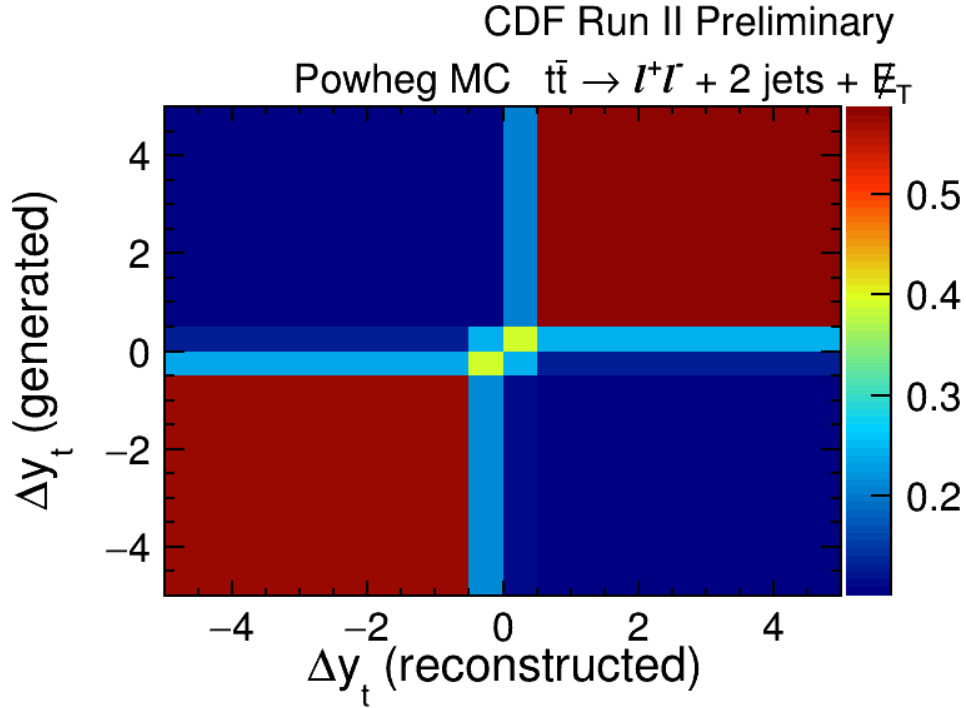


FIG. 6: The detector smearing matrix estimated with the nominal POWHEG MC.

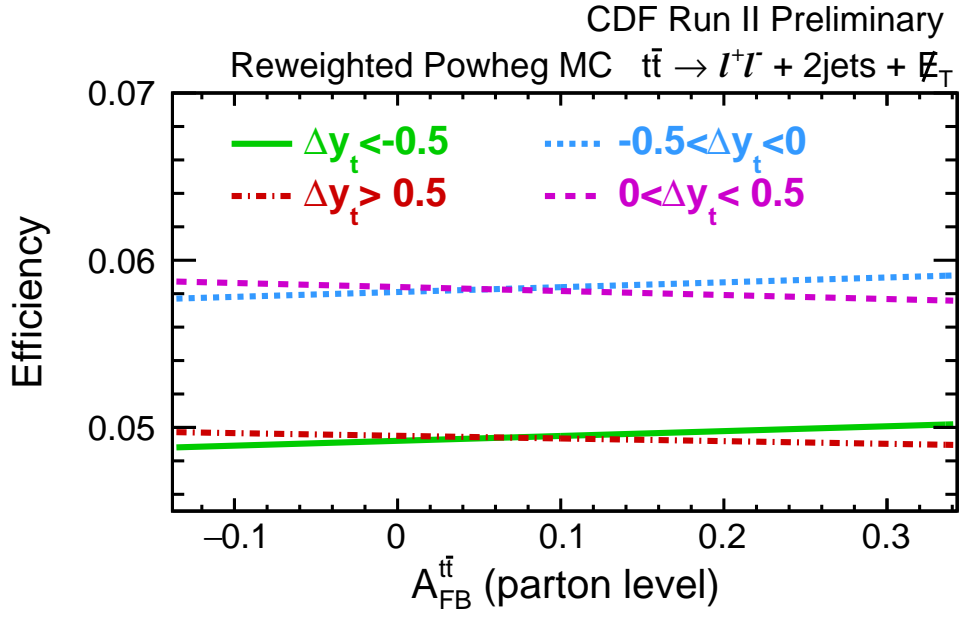


FIG. 7: The efficiencies in the four bins, characterized as linear functions of the $A_{\text{FB}}^{t\bar{t}}$, estimated with the reweighted POWHEG MC sample.

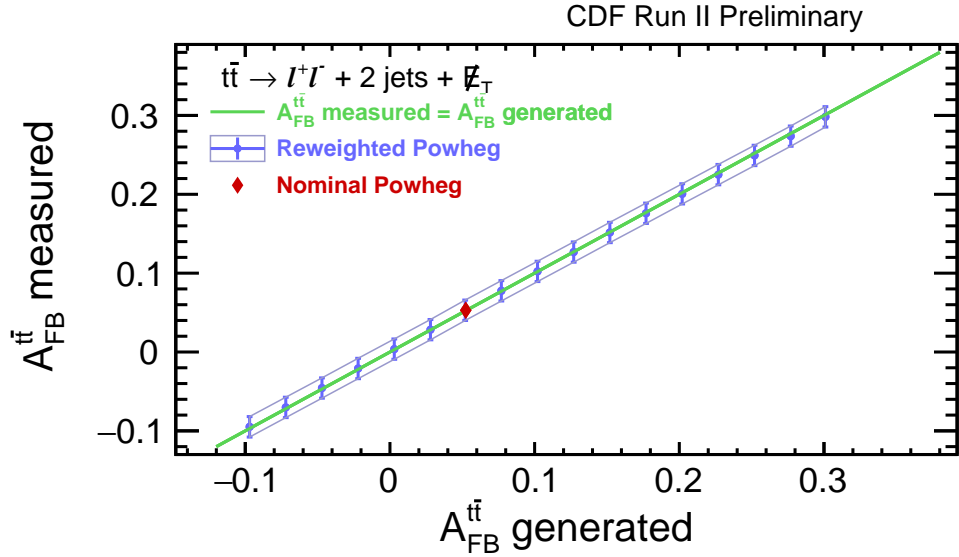


FIG. 8: A comparison of the $A_{\text{FB}}^{t\bar{t}}$ measured with the unfolding algorithm compared with the $A_{\text{FB}}^{t\bar{t}}$ generated, for the reweighted POWHEG MC samples, with $-0.1 < A_{\text{FB}}^{t\bar{t}} < 0.3$. No bias is observed.

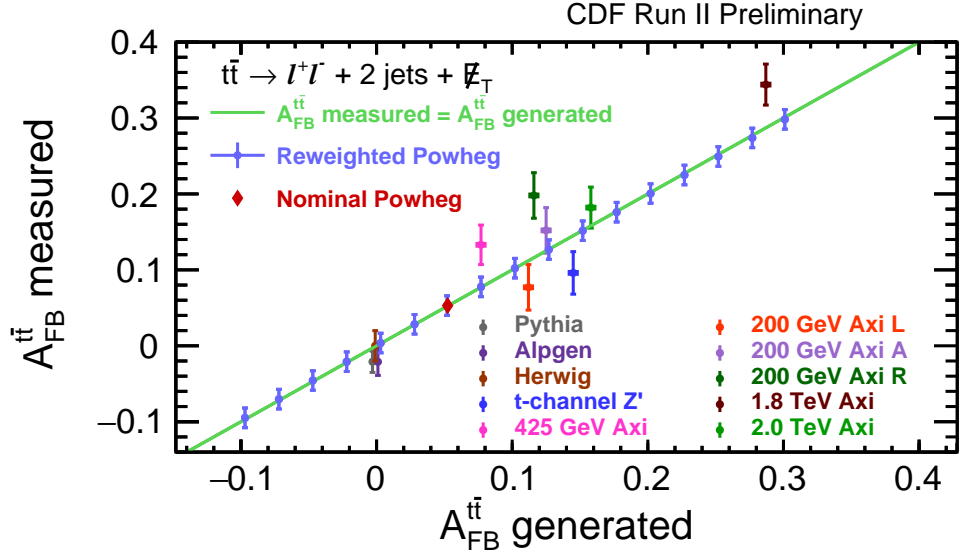


FIG. 9: A comparison of the $A_{\text{FB}}^{t\bar{t}}$ measured with the unfolding algorithm with the $A_{\text{FB}}^{t\bar{t}}$ generated, for the reweighted POWHEG MC samples and benchmark BSM scenarios. We take the difference between the generated $A_{\text{FB}}^{t\bar{t}}$ and the measured $A_{\text{FB}}^{t\bar{t}}$ with the PYTHIA MC sample (0.02) as an unfolding systematic uncertainty.

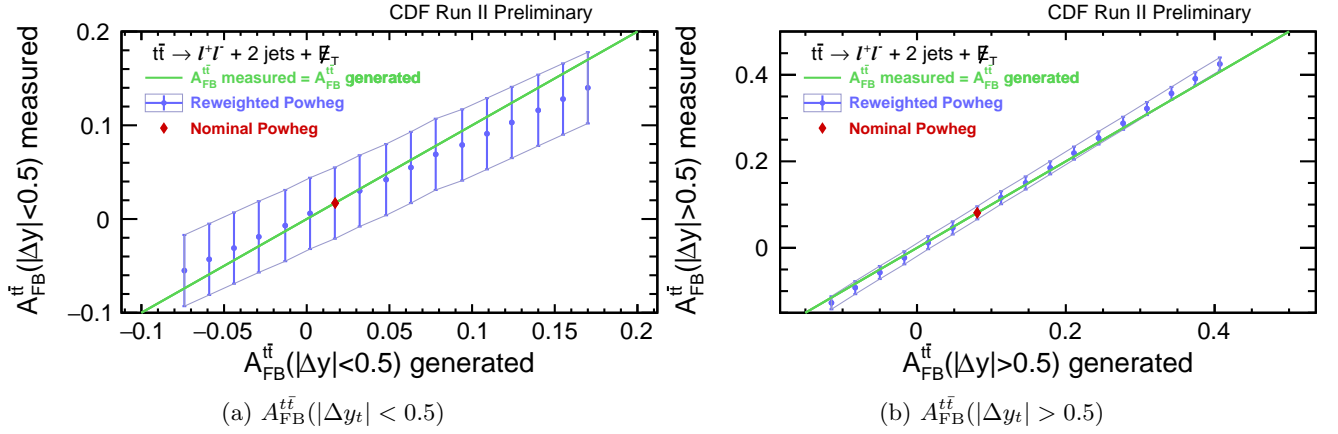


FIG. 10: A comparison of the $A_{\text{FB}}^{t\bar{t}}$ measured with the unfolding algorithm with the $A_{\text{FB}}^{t\bar{t}}$ generated in the two $|\Delta y_t|$ bins, for the reweighted POWHEG MC samples. We note that the uncertainties correspond to the size of the POWHEG MC sample which is over a factor of 100 more than the data, and the measured values are always within 1σ of the generated values. While there does seem to be a visible bias, this could well be a statistical fluctuation since all points are correlated. Rather than correct for what could be a fluctuation and in the worst case negligible compared with the expected statistical uncertainties, we take the deviations as systematic uncertainties.

7. SYSTEMATICS

In addition to the background systematic uncertainty, several systematic uncertainties need to be taken into account. We estimate the unfolding systematics to be the difference between the measured and generated $A_{\text{FB}}^{t\bar{t}}$ from the PYTHIA MC sample as described in Sec. 6. Other systematic uncertainties due to the jet energy scale, modeling of the parton shower, modeling of the color reconnection, modeling of initial- and final-state radiation, and parton distribution functions are estimated in the same way as in the leptonic A_{FB} measurement [12]. Table III summarizes the statistical and systematic uncertainties of the inclusive $A_{\text{FB}}^{t\bar{t}}$ measurement, and Table IV summarizes the uncertainties for the $A_{\text{FB}}^{t\bar{t}}$ vs. $|\Delta y_t|$ measurements.

CDF Run II Preliminary (9.1 fb ⁻¹) ($t\bar{t} \rightarrow l^+l^- + 2\text{jets} + \cancel{E}_T$)	
Source of uncertainty	Value
$A_{\text{FB}}^{t\bar{t}}$	
Statistical	0.11
Background	0.04
Parton Showering	0.03
Color reconnection	0.03
I/FSR	0.03
JES	0.02
Unfolding	0.02
PDF	0.01
Total systematic	0.07
Total uncertainty	0.13

TABLE III: Table of uncertainties for the inclusive $A_{\text{FB}}^{t\bar{t}}$ measurement.

CDF Run II Preliminary (9.1 fb ⁻¹) ($t\bar{t} \rightarrow l^+l^- + 2\text{jets} + \cancel{E}_T$)		
Source of uncertainty	$A_{\text{FB}}^{t\bar{t}}(\Delta y_t < 0.5)$	$A_{\text{FB}}^{t\bar{t}}(\Delta y_t > 0.5)$
Statistical	0.33	0.13
Background	0.13	0.06
Parton Showering	0.07	0.06
Color reconnection	0.12	0.06
I/FSR	0.05	0.03
JES	0.02	0.02
Unfolding	0.06	0.02
PDF	0.01	0.01
Total systematic	0.20	0.11
Total uncertainty	0.39	0.17

TABLE IV: Table of uncertainties for the $A_{\text{FB}}^{t\bar{t}}(|\Delta y_t| < 0.5)$ and $A_{\text{FB}}^{t\bar{t}}(|\Delta y_t| > 0.5)$ measurements.

8. DILEPTON RESULTS

With the data validated, and the procedure vetted and optimized, we open the box. Figure 11 shows the posterior probability density of the inclusive $A_{\text{FB}}^{t\bar{t}}$. A Gaussian function is fitted to the center of the distribution to extract the result. Including the systematic uncertainties summarized in Table III, the parton-level inclusive $A_{\text{FB}}^{t\bar{t}}$ is measured to be

$$A_{\text{FB}}^{t\bar{t}} = 0.12 \pm 0.11(\text{stat.}) \pm 0.07(\text{syst.}) = 0.12 \pm 0.13. \quad (8)$$

Figure 12 shows the comparison between all Tevatron inclusive $A_{\text{FB}}^{t\bar{t}}$ measurements and the NLO/NNLO SM predictions. No obvious deviation is shown.

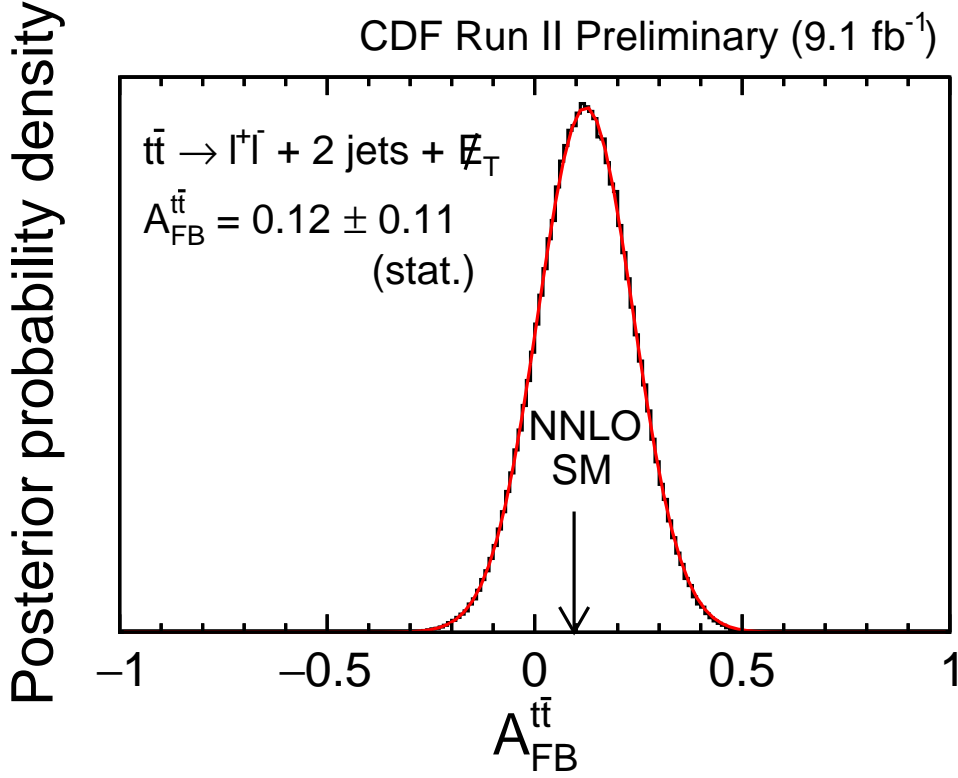


FIG. 11: The posterior probability density for the measurement of the inclusive $A_{\text{FB}}^{t\bar{t}}$. A Gaussian function is fitted to the center of the distribution to extract the result.

Figure 13 shows the posterior probability densities of $A_{\text{FB}}^{t\bar{t}}(|\Delta y_t| < 0.5)$ and $A_{\text{FB}}^{t\bar{t}}(|\Delta y_t| > 0.5)$ with Gaussian functions fitted to the center of the distributions to extract the results. Fig. 14 shows the two-dimensional posterior probability density distribution of $A_{\text{FB}}^{t\bar{t}}$ in the two $|\Delta y_t|$ regions, which indicates that the two measurements are anti-correlated as expected. The correlation between the two observables is estimated to be -0.44. Including the systematic uncertainties summarized in Table IV, the parton-level inclusive $A_{\text{FB}}^{t\bar{t}}$ vs $|\Delta y_t|$ are measured to be

$$A_{\text{FB}}^{t\bar{t}}(|\Delta y_t| < 0.5) = 0.12 \pm 0.33(\text{stat.}) \pm 0.20(\text{syst.}) = 0.12 \pm 0.39, \quad (9)$$

$$A_{\text{FB}}^{t\bar{t}}(|\Delta y_t| > 0.5) = 0.13 \pm 0.13(\text{stat.}) \pm 0.11(\text{syst.}) = 0.13 \pm 0.17. \quad (10)$$

Note that the uncertainty for $|\Delta y_t| < 0.5$ is significantly larger because of the large bin migrations in that region which reduce the statistical power of the data.

To determine the slope, we place our data points at the bin centroids predicted by the POWHEG MC sample and fit the two differential $A_{\text{FB}}^{t\bar{t}}$ results with a linear function with zero intercept, taking all uncertainties with their correlations into account. The resultant slope of the linear fit is $\alpha = 0.14 \pm 0.15$. Figure 15 shows a comparison of $A_{\text{FB}}^{t\bar{t}}$ vs. $|\Delta y_t|$ results of this measurement to other Tevatron measurements [6, 7] as well as the NNLO SM predictions [3, 5]. All results are consistent with each other within statistics.

Tevatron Top Asymmetry

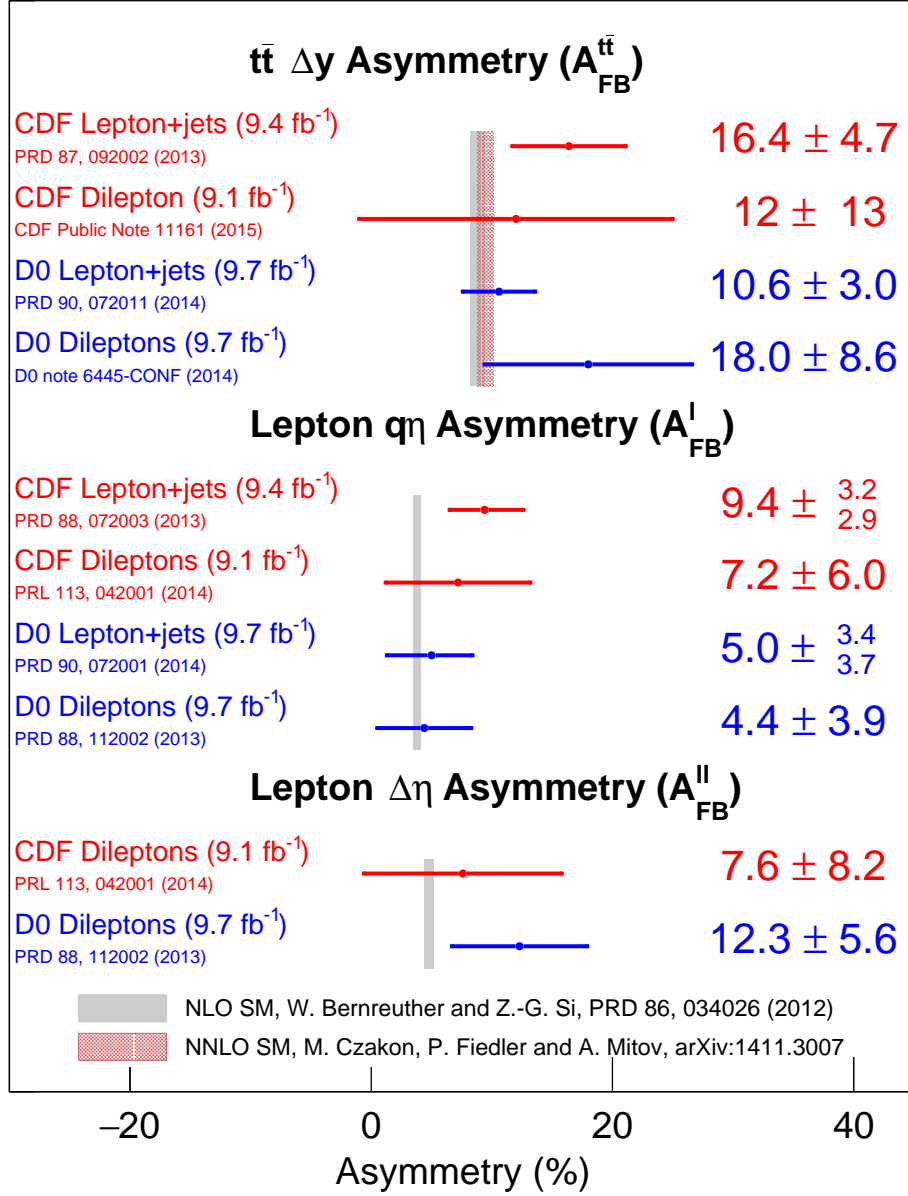


FIG. 12: A comparison of all inclusive top A_{FB} results from the Tevatron with the NLO and NNLO SM predictions.

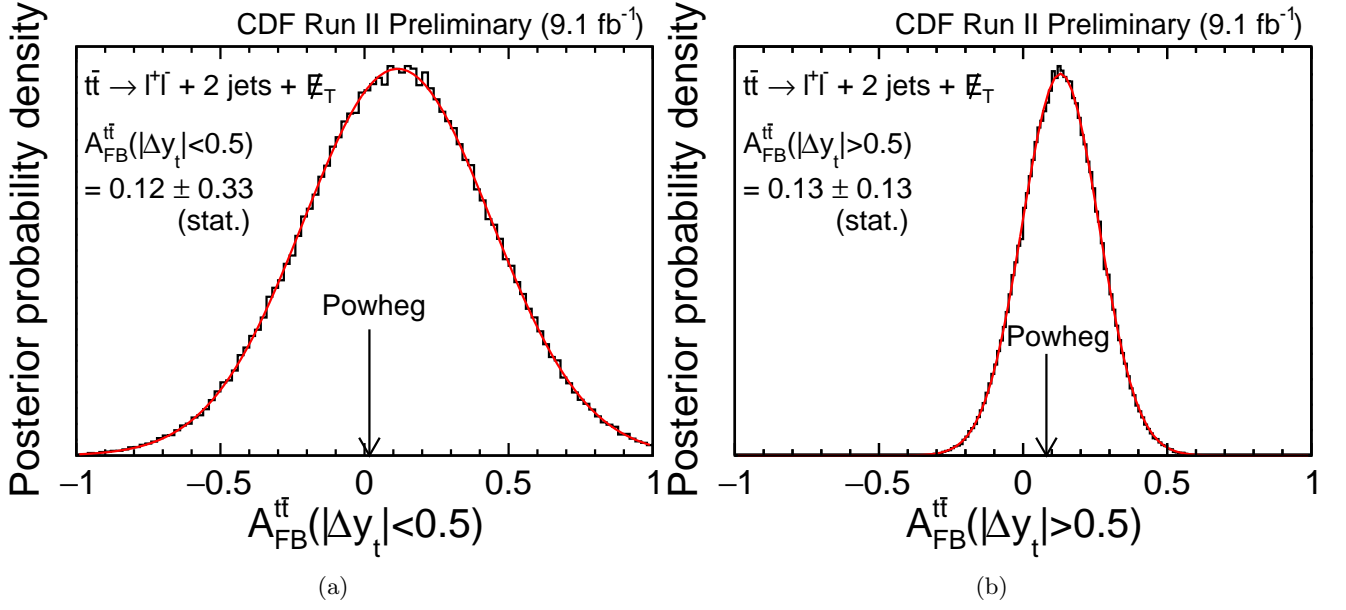


FIG. 13: The posterior probability density distributions of (a) $A_{\text{FB}}^{t\bar{t}}(|\Delta y_t| < 0.5)$ and (b) $A_{\text{FB}}^{t\bar{t}}(|\Delta y_t| > 0.5)$. Gaussian functions are fitted to the center of the distributions to extract the results.

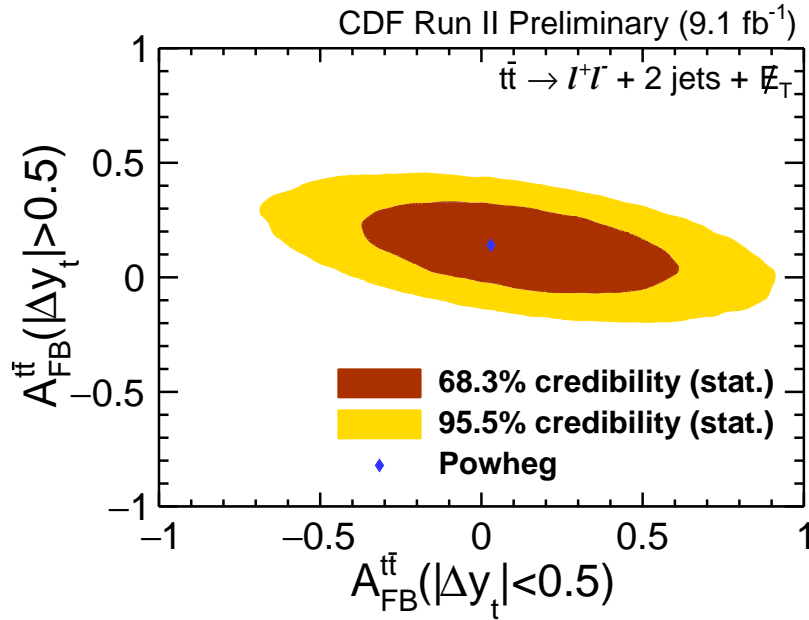


FIG. 14: The 2D posterior probability density distribution of $A_{\text{FB}}^{t\bar{t}}(|\Delta y_t| < 0.5)$ vs. $A_{\text{FB}}^{t\bar{t}}(|\Delta y_t| > 0.5)$. The correlation between the two observables is estimated to be -0.44.

9. CDF COMBINATION OF $A_{\text{FB}}^{t\bar{t}}$ INCLUSIVE AND DIFFERENTIAL $A_{\text{FB}}^{t\bar{t}}$ RESULTS FROM THE DILEPTON AND LEPTON+JETS FINAL STATES

In this section we report the combination of the dilepton results with results in the lepton+jets final state in Ref. [6]. The combination of the inclusive $A_{\text{FB}}^{t\bar{t}}$ is based on the *best linear unbiased estimates* (BLUE)[31]. For the differential slope value, we perform a simultaneous linear fit for the $A_{\text{FB}}^{t\bar{t}}$ as a function of $|\Delta y_t|$ in both final states.

The treatment of the correlations of the statistical and systematic uncertainties between the two measurements is the same as in the CDF combination of the A_{FB}^{ℓ} measurement [12]. We quickly describe the various uncertainties and how they are combined. Since the two measurements are done in orthogonal final states, the statistical uncertainties are taken as uncorrelated. The two measurements share a small portion of the backgrounds, and the backgrounds systematic uncertainties are mainly caused by the uncertainties in the shape of the background Δy_t distributions, which are uncorrelated between the two measurements, thus the background uncertainties are treated as uncorrelated. The correction procedures are different in the two measurements, thus the corresponding uncertainties are treated as uncorrelated. The uncertainties due to the parton shower model, the jet energy scale, the initial- and final-state radiation, the color reconnection model, and the parton-distribution functions are estimated in virtually identical ways, thus they are treated as fully correlated. Table V summarizes the uncertainties and the correlations in both inclusive $A_{\text{FB}}^{t\bar{t}}$ measurements. With these uncertainties and the correlations, the combined $A_{\text{FB}}^{t\bar{t}}$ based on BLUE is

$$A_{\text{FB}}^{t\bar{t}} = 0.160 \pm 0.045. \quad (11)$$

The weights of the lepton+jets result and the dilepton result are 91% and 9%, respectively. The correlation between the two results is 10%. The comparison of the CDF combined inclusive $A_{\text{FB}}^{t\bar{t}}$ with other measurements and SM calculations is shown in Fig. 17a.

CDF Run II Preliminary			
Source of uncertainty	L+J (9.4 fb ⁻¹)	DIL (9.1 fb ⁻¹)	Correlation
Background shape	0.018	0.04	0
Background normalization	0.013		
Parton shower	0.01	0.03	1
Jet energy scale	0.007	0.02	1
Initial- and final-state radiation	0.005	0.03	1
Correction procedure	0.004	0.02	0
Color reconnection	0.001	0.03	1
Parton-distribution functions	0.001	0.01	1
Total systematic	0.026	0.07	
Statistical	0.039	0.11	0
Total uncertainty	0.047	0.13	

TABLE V: Table of uncertainties for $A_{\text{FB}}^{t\bar{t}}$ measurements in the lepton+jets and the dilepton final states and their correlations. In the column of correlation, “0” indicates no correlation and “1” indicates fully positive correlation.

For the differential $A_{\text{FB}}^{t\bar{t}}$, rather than combining the data points we perform a simultaneous fit for the slope α of the differential $A_{\text{FB}}^{t\bar{t}}$ as a function of $|\Delta y_t|$ using both sets of data points (four in lepton+jets final state and two in dilepton final state). The bin-centroids expected by the POWHEG MC and the $A_{\text{FB}}^{t\bar{t}}$ in those bins are summarized in Table VI as well as the eigenvalues and the eigenvectors of the corresponding covariance matrix. The simultaneous fit is obtained by minimizing a χ^2 term defined as

$$\chi^2 = \sum_{i=1}^6 \sum_{j=1}^6 (A_{\text{FB}}^{t\bar{t}}[i] - \alpha \cdot |\Delta y_t|[i]) \cdot \text{Cov}^{-1}[i][j] \cdot (A_{\text{FB}}^{t\bar{t}}[j] - \alpha \cdot |\Delta y_t|[j]), \quad (12)$$

where $|\Delta y_t|[i]$ and $A_{\text{FB}}^{t\bar{t}}[i]$ are the i -th bin centroids and the $A_{\text{FB}}^{t\bar{t}}(|\Delta y_t|)$ shown in Table VI respectively, $\text{Cov}^{-1}[i][j]$ is the corresponding element of the inverse matrix of the covariance matrix whose eigenvalues and eigenvectors are also shown in Table VI, and α is the slope we are fitting for. The result is found to be $\alpha = 0.227 \pm 0.057$, which is 2.0σ above the NNLO SM prediction. A comparison of the data as a function of Δy_t , along with other results and the SM prediction, is shown in Figs 16 and 17b.

CDF Run II Preliminary

		Bin centroid $ \Delta y_t $	$A_{\text{FB}}^{t\bar{t}}$ (Δy_t)	Covariance matrix						
				λ	0.156	0.0296	0.0251	0.00732	0.000682	0.000476
L+J	$ \Delta y_t < 0.5$	0.24	0.048	Eigenvectors	-0.018	0.064	-0.012	-0.371	0.904	-0.201
	$0.5 < \Delta y_t < 1.0$	0.73	0.180		0.001	-0.030	-0.014	-0.840	-0.235	0.487
	$1.0 < \Delta y_t < 1.5$	1.22	0.356		0.008	-0.440	-0.172	-0.344	-0.281	-0.761
	$ \Delta y_t > 1.5$	1.82	0.477		0.030	-0.830	-0.286	0.193	0.219	0.378
DIL	$ \Delta y_t < 0.5$	0.24	0.11		-0.984	-0.087	0.155	0.005	-0.008	0.006
	$ \Delta y_t > 0.5$	1.01	0.13		0.174	-0.322	0.930	-0.023	0.024	-0.021

TABLE VI: Bin centroids and the differential $A_{\text{FB}}^{t\bar{t}}$ in the $A_{\text{FB}}^{t\bar{t}}$ vs. $|\Delta y_t|$ measurements in both the lepton+jets and the dilepton final states as well as the corresponding eigenvalues and eigenvectors of the covariance matrix.

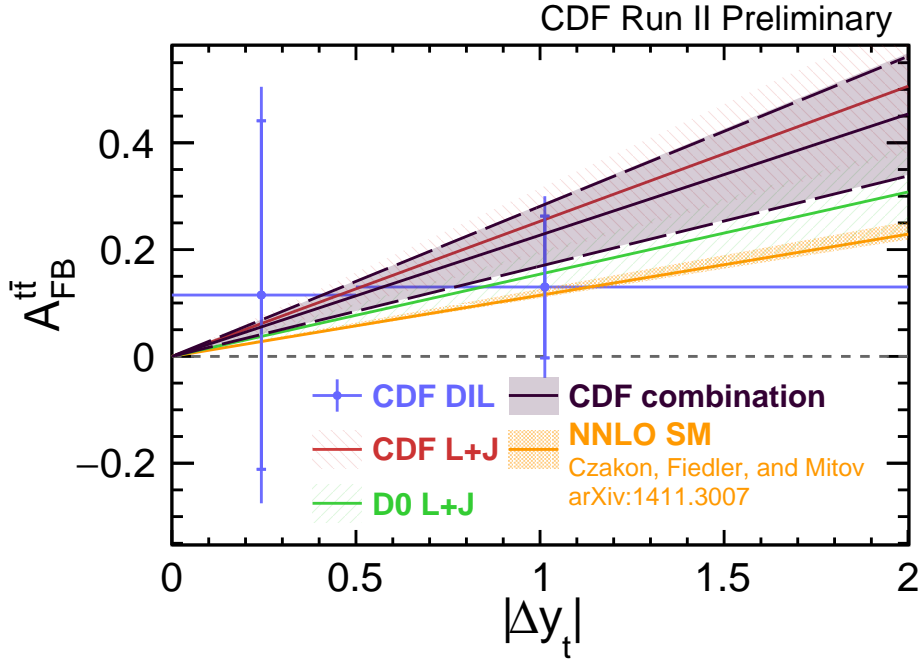
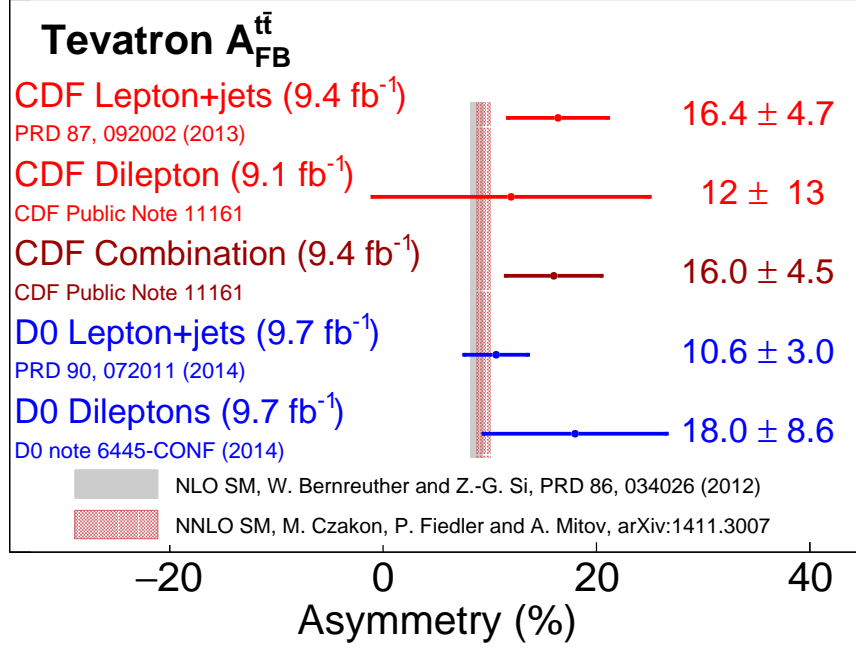
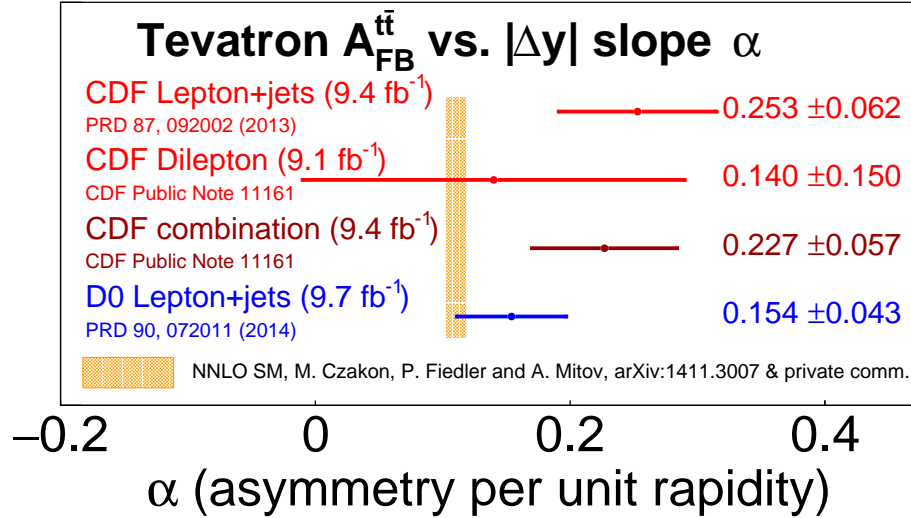


FIG. 16: A comparison of the simultaneous fit for the slope α in both the lepton+jets and the dilepton final states with other Tevatron measurements as well as the NNLO SM predictions [3, 5].



(a)



(b)

FIG. 17: Comparison of the combined inclusive $A_{\text{FB}}^{t\bar{t}}$ and the slope α of $A_{\text{FB}}^{t\bar{t}}$ vs. $|\Delta y|$ with measurements in the lepton+jets and dilepton final states from CDF [6], in the lepton+jets final state from D0 [7], and the NLO [1] and NNLO [3, 5] SM calculations.

10. CONCLUSION

We have measured both the inclusive and the differential values of the parton-level inclusive $A_{\text{FB}}^{t\bar{t}}$ in the dilepton final state and combined them with the results from CDF in the lepton+jets final state. The results from the dilepton final state are $A_{\text{FB}}^{t\bar{t}} = 0.12 \pm 0.11(\text{stat.}) \pm 0.07(\text{syst.}) = 0.12 \pm 0.13$, $A_{\text{FB}}^{t\bar{t}}(|\Delta y_t| < 0.5) = 0.12 \pm 0.33(\text{stat.}) \pm 0.20(\text{syst.}) = 0.12 \pm 0.39$, and $A_{\text{FB}}^{t\bar{t}}(|\Delta y_t| > 0.5) = 0.13 \pm 0.13(\text{stat.}) \pm 0.11(\text{syst.}) = 0.13 \pm 0.17$. A linear fit with zero intercept to the differential $A_{\text{FB}}^{t\bar{t}}$ as a function of $|\Delta y_t|$ yields a slope of $\alpha = 0.14 \pm 0.15$. All the results are consistent with the previous measurements. After combination, the legacy measurement at CDF for the inclusive $A_{\text{FB}}^{t\bar{t}}$ at CDF yields a value of $A_{\text{FB}}^{t\bar{t}} = 0.160 \pm 0.045$, which is consistent with the NNLO SM prediction within 1.5σ . The simultaneous linear fit for the $A_{\text{FB}}^{t\bar{t}}$ as a function of $|\Delta y_t|$ with zero intercept yields a slope of $\alpha = 0.227 \pm 0.057$, which is 2σ higher than the NNLO SM prediction [3, 5].

ACKNOWLEDGMENTS

We thank the Fermilab staff and the technical staffs of the participating institutions for their vital contributions. This work was supported by the U.S. Department of Energy and National Science Foundation; the Italian Istituto Nazionale di Fisica Nucleare; the Ministry of Education, Culture, Sports, Science and Technology of Japan; the Natural Sciences and Engineering Research Council of Canada; the National Science Council of the Republic of China; the Swiss National Science Foundation; the A.P. Sloan Foundation; the Bundesministerium für Bildung und Forschung, Germany; the Korean World Class University Program, the National Research Foundation of Korea; the Science and Technology Facilities Council and the Royal Society, United Kingdom; the Russian Foundation for Basic Research; the Ministerio de Ciencia e Innovación, and Programa Consolider-Ingenio 2010, Spain; the Slovak R&D Agency; the Academy of Finland; the Australian Research Council (ARC); and the EU community Marie Curie Fellowship Contract No. 302103.

-
- [1] W. Bernreuther and Z.-G. Si, Phys. Rev. **D 86**, 034026 (2012).
- [2] J. A. Aguilar-Saavedra, D. Amidei, A. Juste, and M. Pérez-Victoria, Rev. Mod. Phys. **87**, 421 (2015).
- [3] M. Czakon, P. Fiedler, and A. Mitov, arXiv:1411.3007 [hep-ph].
- [4] D.-W. Jung, P. Ko, and J. S. Lee, Phys. Lett. **B 701**, 248 (2011); D.-W. Jung, P. Ko, J. S. Lee, and S. hyeon Nam, *ibid.* **691**, 238 (2010); E. Álvarez, L. Rold, and A. Szykman, J. High Energy Phys. 05 (2011) 070; C.-H. Chen, G. Cvetic, and C. Kim, Phys. Lett. **B 694**, 393 (2011); Y.-k. Wang, B. Xiao, and S.-h. Zhu, Phys. Rev. **D 82**, 094011 (2010); A. Djouadi, G. Moreau, F. m. c. Richard, and R. K. Singh, *ibid.* **82**, 071702 (2010); R. S. Chivukula, E. H. Simmons, and C.-P. Yuan, *ibid.* **82**, 094009 (2010); B. Xiao, Y.-k. Wang, and S.-h. Zhu, *ibid.* **82**, 034026 (2010); Q.-H. Cao, D. McKeen, J. L. Rosner, G. Shaughnessy, and C. E. M. Wagner, *ibid.* **81**, 114004 (2010); I. Doršner, S. Fajfer, J. F. Kamenik, and N. Košnik, *ibid.* **81**, 055009 (2010); S. Jung, H. Murayama, A. Pierce, and J. D. Wells, *ibid.* **81**, 015004 (2010); J. Shu, T. M. P. Tait, and K. Wang, *ibid.* **81**, 034012 (2010); A. Arhrib, R. Benbrik, and C.-H. Chen, *ibid.* **82**, 034034 (2010); J. Cao, Z. Heng, L. Wu, and J. M. Yang, *ibid.* **81**, 014016 (2010); V. Barger, W.-Y. Keung, and C.-T. Yu, *ibid.* **81**, 113009 (2010); P. Ferrario and G. Rodrigo, *ibid.* **78**, 094018 (2008); **80**, 051701 (2009); M. Bauer, F. Goertz, U. Haisch, T. Pfoh, and S. Westhoff, J. High Energy Phys. 11 (2010) 039; K. Cheung, W.-Y. Keung, and T.-C. Yuan, Phys. Lett. **B 682**, 287 (2009).
- [5] M. Czakon, P. Fiedler, and A. Mitov, Private communication.
- [6] T. Aaltonen *et al.* (CDF Collaboration), Phys. Rev. **D 87**, 092002 (2013).
- [7] V. Abazov *et al.* (D0 Collaboration), Phys.Rev. **D90**, 072011 (2014).
- [8] V. Abazov *et al.* (D0 Collaboration), D0 Note 6445-CONF (2014).
- [9] T. Aaltonen *et al.* (CDF Collaboration), Phys. Rev. Lett. **111**, 182002 (2013).
- [10] W. Bernreuther and Z.-G. Si, Nuclear Physics B **837**, 90 (2010).
- [11] T. Aaltonen *et al.* (CDF Collaboration), CDF Public Note 10436.
- [12] T. Aaltonen *et al.* (CDF Collaboration), Phys.Rev.Lett. **113**, 042001 (2014).
- [13] S. Alioli, S.-O. Moch, and P. Uwer, J. High Energy Phys. 01 (2012) 137; P. Nason, J. High Energy Phys. 11 (2004) 040; S. Frixione, P. Nason, and C. Oleari, J. High Energy Phys. 11 (2007) 070; S. Alioli, P. Nason, C. Oleari, and E. Re, J. High Energy Phys. 06 (2010) 043.
- [14] E. Gerchtein and M. Paulini, eConf **C0303241**, TUMT005 (2003).
- [15] A. Bhatti *et al.*, Nucl. Instrum. Meth. A **566**, 375 (2006).
- [16] A. Abulencia *et al.* (CDF Collaboration), Phys. Rev. **D 73**, 112006 (2006).
- [17] K. Olive *et al.* (Particle Data Group), Chin.Phys. **C38**, 090001 (2014).
- [18] N. Metropolis *et al.*, The Journal of Chemical Physics **21**, 1087 (1953).
- [19] A. Caldwell, D. Kollr, and K. Krniger, Computer Physics Communications **180**, 2197 (2009).
- [20] T. Aaltonen *et al.* (CDF Collaboration), Phys. Rev. **D 88**, 032003 (2013).
- [21] T. Aaltonen *et al.* (CDF Collaboration), arXiv:1504.06888 [hep-ex].
- [22] J. Antos, Acta Phys.Slov. **58**, 155 (2008).
- [23] T. Aaltonen *et al.* (CDF collaboration), arXiv:1505.00500 [hep-ex].
- [24] T. Sjostrand, S. Mrenna, and P. Z. Skands, J. High Energy Phys. 05 (2006) 026.
- [25] M. L. Mangano, M. Moretti, F. Piccinini, R. Pittau, and A. D. Polosa, J. High Energy Phys. 07 (2003) 001.
- [26] M. Bahr, S. Gieseke, M. Gigg, D. Grellscheid, K. Hamilton, *et al.*, Eur.Phys.J. **C 58**, 639 (2008).
- [27] S. Jung, A. Pierce, and J. D. Wells, Phys. Rev. **D 83**, 114039 (2011).
- [28] G. Marques Tavares and M. Schmaltz, Phys. Rev. **D 84**, 054008 (2011).
- [29] A. Falkowski, M. L. Mangano, A. Martin, G. Perez, and J. Winter, Phys. Rev. **D 87**, 034039 (2013).
- [30] T. Aaltonen *et al.* (CDF Collaboration), Phys. Rev. **D 83**, 112003 (2011).
- [31] L. Lyons, D. Gibaut, and P. Clifford, Nucl. Instrum. Meth. A **270**, 110 (1988); L. Lyons, A. J. Martin, and D. H. Saxon, Phys. Rev. **D 41**, 982 (1990); A. Valassi, Nucl. Instrum. Meth. A **500**, 391 (2003).